Computing ischemic regions in the heart with the bidomain model; first steps towards validation

Bjørn Fredrik Nielsen, Marius Lysaker and Per Grøttum

***Abstract*—We investigate whether it is possible to use the bidomain model and body surface potential maps (BSPMs) to compute the size and position of ischemic regions in the human heart. This leads to a severely ill posed inverse problem for a potential equation. We do not use the classical inverse problems of electrocardiography, in which the unknown sources are the epicardial potential distribution or the activation sequence. Instead we employ the bidomain theory to obtain a model that also enables identification of ischemic regions transmurally. This approach makes it possible to distinguish between subendocardial and transmural cases, only using the BSPM data.**

The main focus is on testing a previously published algorithm on clinical data, and the results are compared with images taken with perfusion scintigraphy. For the four patients involved in this study, the two modalities produce results that are rather similar: The relative differences between the center of mass and the size of the ischemic regions, suggested by the two modalities, are $10.8\% \pm 4.4\%$ and $7.1\% \pm 4.6\%$, respectively. We also present some simulations which indicate that the methodology is robust with respect to uncertainties in important model parameters. However, in contrast to what has been observed in investigations only involving synthetic data, inequality constraints are needed to obtain sound results.

***Index Terms*—Electrophysical imaging, heart, inverse methods.**

I. Introduction

The electrocardiogram remains the recommended and most used screening tool for diagnosis and risk stratification of angina pectoris and myocardial infarction [1]–[4]. It has, however, several shortcomings; in 12-lead exercise testing the most important are low sensitivity (50-68%) for diagnosing coronary artery disease [3], [4], inability to locate the ischemic lesion from the distribution of ST-segment depressions [5]–[8], and uncertain relation between the size of ST-segment depressions and angiographic or scintigraphic indices of disease severity [6], [8]–[12].

This work was supported by the Norwegian Research Council through the grant 182580 "ECG Analyzer - Demonstrating the viability of mathematical methods for early diagnosis of heart infarction".

Bjørn Fredrik Nielsen is with Simula Research Laboratory and the Center for Cardiological Innovation, Oslo University Hospital, Norway. He is also Professor of Applied Mathematics at Department of Mathematical Sciences and Technology, Norwegian University of Life Sciences, P.O. Box 5003, 1432 Aas, Norway (e-mail: bjorn.f.nielsen@umb.no).

Marius Lysaker is with Simula Research Laboratory and the Center for Cardiological Innovation, Oslo University Hospital, Norway. He is also Associate Professor of Applied Mathematics at Faculty of Technology, Telemark University College, P.O. Box 203, 3901 Porsgrunn, Norway (e-mail: marius.lysaker@hit.no).

Per Grøttum is Professor of Medicine at Faculty of Medicine, University of Oslo, P.O. Box 1078, 0316 Oslo, Norway (e-mail: per@medisin.uio.no).

Simple amplitude measurements are still the basis for the interpretation of the exercise ECG, e.g., the diagnostic criterion of 1mm flat ST-depression was established in 1957 [13]. Although more advanced processing of the exercise electrocardiogram has been attempted [14]–[16], none has gained widespread use. In 1997 Oster et al. introduced the term "ECG imaging" [17] to describe a system that could depict detailed spatial and temporal information about the electrical activity of the heart from body surface measurements, providing the user with the visual advantages of imaging modalities. To achieve this, an inverse solution of the potential equation must be computed, which is a mathematically severely ill posed problem that requires skillful regularization to provide a stable solution [18]–[20]. So far, mainly epicardial potentials [21]–[27] and activation sequences [28]–[32] have been computed. For these two source formulations, a number of impressive validation studies have been published, see e.g. [17], [27], [30], [33]–[37], [38]–[41] and references therein.

Clinically, these methods have been used to assess activation patterns during arrhythmias [33], [34], [36], activation patterns in CRT-treated congestive heart failure [35], and the location of infarct-related myocardial scars [37]. Ischemia has been assessed by epicardial potential reconstruction, quantitatively in dogs [41], and qualitatively in man during PCI [40].

To our knowledge Li and He [42] published the first method for full transmural assessment of ischemia, based on artificial neural networks. We have later developed and shown that a full transmural static bidomain model can detect the location and size of simulated ischemia [43]–[46], which has been confirmed in a recent study by Wang et al. [47]. The purpose of the present study is to examine, in a small and highly selected group of patients with coronary heart disease, whether this method can be extended to full 3D use in a common clinical setting, namely exercise-induced ischemia. So far the technology has only been tested on four patients. Although the results are rather promising, far more tests are needed in order to validate the clinical value of solving this inverse problem. Our findings provide a proof-of-concept and show that a complete validation might turn out successfully.

As briefly mentioned above, detailed information about the voltage distribution in the myocardium from ECGs can also be computed by artificial neural networks. This promising approach has been studied in a number of by papers by He et al. [42], [48], [49]. Furthermore, the validation issue has been thoroughly addressed [50], including the possibility of computing transmural extracellular potentials [51]. In the present study we do not use artificial neural networks, but a method based on the bidomain model.

II. Method

A. Patients

Four male patients, age range 62-81 years, were included in the study. The patients were recruited from the population referred to and accepted for coronary evaluation at Oslo University Hospital on the suspicion of coronary artery disease. All patients had exercise induced angina, positive exercise ECGs and positive myocardial perfusion scintigrams during exercise. Patients 1 and 2 had previous myocardial infarctions, patients 3 and 4 had no previous heart disease.

B. Myocardial scintigraphy

The patients underwent 99mTc-Tetrofosmin SPECT myocardial scintigraphy using a one-day (rest-stress) protocol. A body weight dependent dose of 99mTc-Tetrofosmin (Myoview), e.g. 300 MBeq for 70-100 kg weight, was used in the rest study. The stress test was performed on an ergometer bicycle with a ramp-up protocol of 25 W every minute until symptoms appeared or 85% of age-adjusted expected maximal heart rate was achieved or the patient was nearly exhausted. Three times the resting dose of 99mTc-Tetrofosmin was subsequently injected and the patient continued to bicycle at the same or a slightly reduced load for 2 minutes. Scintigraphy was performed 1 hour later. The images were analyzed on a General Electric Xeleris system using the 4DMSPECT package. Counts were normalized automatically by the hottest pixel technique. The basal cardiac plane was set manually to correspond to that of the MR reconstruction (see later). Polar plots of the count ratios between the stress and rest images were computed.

C. Body surface potential maps/electrocardiograms

Body surface potential maps (BSPM[1]) were recorded during the exercise test with a BioSemi ActiveTwo system [52], employing 72 leads. 64 leads were organized as 4 equidistant, vertical strips each of 8 electrodes on the thorax and the same on the back. In addition, 4 vertical, axillar leads were added on each side. The standard Wilson central terminal was used as reference. Signals were digitized at 2kHz per channel without filtering. From the recordings a baseline sample of 180 seconds (median) was extracted at rest as well as a 60 sec sample starting at the time when 99mTc-Tetrofosmin was injected at maximum exercise. It was assumed that the latter would make the BSPM and the scintigram represent the same ischemia.

Post-processing was performed to measure the ST-segment changes. First 50Hz powerline noise was removed by FFT filtering. QRS templates were then generated in a two-pass process with detection of peaks in the standard deviation as the initial step. Beat detection was subsequently performed by moving-window cross-correlation. Baseline drift was removed by employing cubic spline techniques. QRS onset and the J-point was detected by means of a spatial velocity function. For each beat, the ST-deviation was measured as the average amplitude in the interval J+50msec to J+75msec, and the median[2] of these averages was taken as the ST-segment shift for the selected sample of beats. Finally, for each of the 72 electrodes the ischemia was assessed as the difference between the ST-segment shift in the exercise sample and in the baseline sample.

[1]We will use the terms BSPM and ECG synonymously, i.e. ECG does not refer to the standard 12 lead procedure.

D. Magnetic resonance imaging

Magnetic resonance imaging (MRI) of the torso and the heart was performed with a Siemens 1.5 T machine. Before the examination, cod liver oil pills were taped on the torso in the positions of the BSPM electrodes.

Two sets of MR images were recorded for each patient. One set of images were recorded perpendicularly to the longitudinal axis of the body with a distance of approximately 1.5 cm between the slices. For each image in this set, trained personnel manually identified/marked points along the outer contours of the lungs, the electrode positions and the outer contour of the torso. The other set of images was recorded perpendicularly to the longitudinal axis of the heart. The distance between the slices was approximately 1.0 cm. The basal cardiac plane was identified as the most cranial slice showing both the entire right and left ventricular walls. For each image in this set, the endocardial and epicardial contours of the heart were manually segmented.

E. Geometry and fiber structure

A patient specific geometrical model of the human body was generated from the MR images. Organ by organ, the manually identified points were used to generate spline curves, and the spline curves were transformed to smooth surface models by a technique called lofting [53]. Finally, these surface models were employed to produce a tetrahedrazation by a commercial software package [54].

In order to assemble the complete torso model shown in Figure 1, we need to take into account that the two sets of MR images were recorded from different angles. The heart must be transformed into the coordinate system of the torso data. The MR-scanner provided us with rotational information together with scaling. This means that the orientation and size of the heart was known. However, the actual positioning of the heart was done by hand. As a guide in this process, we computed cross-sectional images of the assembled model and compared them with the torso data by visual inspection.

It is a delicate issue to determine which organs that should be included in the geometrical model of the patients. This matter has been thoroughly studied for forward simulations, see [55] and references therein. Nevertheless, due to the significant amount of noise in clinical BSPMs, it is challenging to assess the level of detailedness required. For the sake of practical reasons, and because of the rather low quality of our MR images, we restricted ourselves to model the torso, lungs and heart with ventricles.

We also designed a myocardial fiber structure to implement anisotropy in the heart model. The fibers are oriented in

[2]The median was used because it is considerably more robust to measurement outliers than the mean. In an exercise situation, with periods of heavy noise in some channels, it is important to choose a robust estimator.

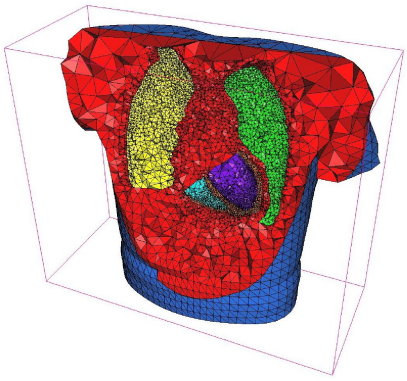

Figure 1. A mesh of the human torso, including lungs and heart with ventricles. (The colors are only used to visualize the ventricles, lungs and the body surface.)

the tangential plane of the ventricles with an angle to the horizontal plane (of the heart) that varies linearly from -60 degrees on the endocardial surface to +60 degrees on the epicardium [56], [57].

F. Inverse solution

We have previously suggested mathematical models and numerical algorithms for the inverse problem of electrocardiography in which ischemic regions are the unknown source. These schemes work almost perfectly on synthetic data. Unfortunately, and to our surprise, it turned out that none of these methods worked on clinical data. The level set approach [43], [44], [58] did not converge, and the fine resolution procedure studied in [45] also failed. These algorithms do not work on patient data because of the amount of noise in the BSPM recordings. This was also confirmed by simulations with synthetic data, by decreasing the signal to noise ratio.

In order to get sound results with clinical data we had to

- introduce inequality constraints,
- discretize the source term on a coarse mesh,
- normalize the exercise ECGs with BSPMs recorded during rest.

Due to these significant changes, we will now present a rather detailed description of our inversion procedure.

1) Bidomain model: Our method for computing ischemic regions in the heart is based on the bidomain model [19], [20], [59] of the electrical activity in the myocardium:

$$\frac{\partial s}{\partial t} = F(s,v) \quad \text{in } H, \tag{1}$$

$$\chi C \frac{dv}{dt} + \chi I(s,v) = \nabla\cdot(\sigma_i\nabla v) + \nabla\cdot(\sigma_i\nabla\phi) \text{ in } H, \tag{2}$$

$$\nabla\cdot(\sigma_i\nabla v) + \nabla\cdot((\sigma_i+\sigma_e)\nabla\phi) = 0 \text{ in } H, \tag{3}$$

where

- F and I are given functions,
- the exact form of F depends on the cell model in use, see e.g. [19], [20] for details,
- I is the total ionic current term, i.e. the sum of the ionic currents, see e.g. [20],
- s is a state vector incorporating ionic currents and gating variables,
- v is the transmembrane potential,
- ϕ is the extracellular potential,
- σ_i and σ_e are the intracellular and extracellular conductivity tensors, respectively,
- H is the domain of the heart,
- χ is the area of cell membrane per unit volume,
- and C is the capacitance of the cell membrane.

With the currently available computing power, it is not possible to use the complete bidomain model to estimate ischemic volumes from ECGs. We thus need a simplified set of equations. In the present framework this was accomplished by combining (3) with biomedical knowledge. More specifically, we exploit the observation that the transmembrane potential v is approximately piecewise constant throughout the myocardium during certain time intervals of the heart cycle. More specifically, v is almost piecewise constant during the plateau and resting phases of a heart beat. Furthermore, the properties of v depend on whether ischemic tissue is present.

Using mathematical symbols, this may be expressed as follows. Let t_1 and t_2 be time instances during the plateau and resting states of the transmembrane action potential, respectively. Previous studies [60]–[64] suggest that reasonable choices for short-lasting, exercise-induced injury may be

$$v(x,t_1) \approx \begin{cases} 20\text{mV} & x \text{ in healthy tissue,} \\ -20\text{mV} & x \text{ in ischemic tissue} \end{cases} \tag{4}$$

and

$$v(x,t_2) \approx \begin{cases} -80\text{mV} & x \text{ in healthy tissue,} \\ -70\text{mV} & x \text{ in ischemic tissue.} \end{cases} \tag{5}$$

From (4) and (5) we conclude that

$$\begin{aligned} h_1(x) &= v(x,t_1) - v(x,t_2) \\ &\approx \begin{cases} 100\text{mV} & x \text{ in healthy tissue,} \\ 50\text{mV} & x \text{ in ischemic tissue.} \end{cases} \end{aligned} \tag{6}$$

We would like to emphasize that the values 100mV and 50mV in (6) have been derived from the measured values presented in (4)-(5), cf. [60]–[64].

In this paper we will refer to h_1 as the shift in the transmembrane potential. The associated ST shift r_1 in the extracellular potential ϕ is defined as the difference between the plateau and resting values of ϕ:

$$r_1(x) = \phi(x,t_1) - \phi(x,t_2). \tag{7}$$

Since (3) must hold for $t = t_1$, t_2, it follows that

$$\begin{aligned} &\nabla\cdot(\sigma_i(x)\nabla v(x,t_1)) \\ &\quad +\nabla\cdot((\sigma_i(x)+\sigma_e(x))\nabla\phi(x,t_1)) = 0 \text{ in } H \end{aligned} \tag{8}$$

and

$$\begin{aligned} &\nabla\cdot(\sigma_i(x)\nabla v(x,t_2)) \\ &\quad +\nabla\cdot((\sigma_i(x)+\sigma_e(x))\nabla\phi(x,t_2)) = 0 \text{ in } H. \end{aligned} \tag{9}$$

By subtracting (9) from (8) we conclude that

$$\nabla\cdot((\sigma_i+\sigma_e)\nabla r_1) = -\nabla\cdot(\sigma_i\nabla h_1) \quad \text{in } H, \tag{10}$$

where h_1 is defined in (6).

We focus on exercise-induced ischemia. The derivation presented above therefore applies to the potential distribution in the patient's heart during exercise testing. As mentioned earlier, the ECGs recorded during exercise were normalized with respect to data acquired at rest. We thus also need a model for the latter situation, which may be obtained as follows: Assume that there are no perfusion anomalies in the patient's myocardium, that is

$$v(x,t) = \begin{cases} 20\text{mV} & t = t_1, \text{ for all } x \in H, \\ -80\text{mV} & t = t_2, \text{ for all } x \in H \end{cases}$$

and the associated shift becomes

$$h_2(x) = v(x,t_1) - v(x,t_2) = 100\text{mV} \quad \text{for all } x \in H. \tag{11}$$

By defining

$$r_2(x) = \phi(x,t_1) - \phi(x,t_2),$$

we obtain an equation corresponding to (10)

$$\nabla \cdot ((\sigma_i + \sigma_e)\nabla r_2) = -\nabla \cdot (\sigma_i \nabla h_2) \quad \text{in } H. \tag{12}$$

Equations (10) and (12) are models of the shifts in the transmembrane and extracellular potentials during exercise and rest, respectively. A model for the difference between these two states is simply obtained by subtracting (10) from (12):

$$\nabla \cdot ((\sigma_i + \sigma_e)\nabla r) = -\nabla \cdot (\sigma_i \nabla h) \quad \text{in } H, \tag{13}$$

where

$$r(x) \quad = \quad r_2(x) - r_1(x)$$

and, see (6) and (11),

$$\begin{aligned} h(x) \quad &= \quad h_2(x) - h_1(x) \\ &= \quad \begin{cases} 0\text{mV} & x \text{ in healthy tissue}, \\ 50\text{mV} & x \text{ in ischemic tissue}. \end{cases} \end{aligned}$$

Keep in mind that (13) only is valid in the heart H.

Outside the heart H, i.e. in the torso T, we assume that there are no sources. This means that the shift r is governed by a standard homogeneous potential equation:

$$\nabla \cdot (\sigma_o \nabla r) = 0 \quad \text{in } T, \tag{14}$$

where σ_o represents the conductivity in T. Throughout this text we will assume that the body is insulated.

To summarize, the shifts r and h are modeled by (13) in the heart H and by (14) in the torso T. Let $B = \overline{H} \cup T$ denote the volume occupied by the body. Combining these facts with suitable conditions at the heart-torso interface and Gauss' divergence theorem, yield the variational form of the model [43]: Find[3] $r \in V$ such that

$$\int_B \nabla\psi \cdot (\sigma \nabla r)\, dx = -\int_H \nabla\psi \cdot (\sigma_i \nabla h)\, dx \quad \text{for all } \psi \in V, \tag{15}$$

[3]Here, $V = H^1(B)$, where $H^1(B)$ is the classical Sobolev space of square integrable functions defined on the body B with square integrable distributional derivatives.

where

$$\sigma(x) = \begin{cases} \sigma_i(x) + \sigma_e(x) & \text{for } x \in H, \\ \sigma_o(x) & \text{for } x \in T, \end{cases} \tag{16}$$

$$h(x) = \begin{cases} 0\text{mV} & x \text{ in healthy tissue}, \\ 50\text{mV} & x \text{ in ischemic tissue}. \end{cases} \tag{17}$$

We assume that the conductivities σ_i, σ_e and σ_o are unaffected by the presence of ischemic tissue. This is a reasonable assumption because we consider exercised induced ischemia and not (old) scars.

If the position, size and shape of the ischemic region is known, then we can define h according to (17) and use (15)-(16) to simulate the ST shift in the body B. In particular, the effects on the ECG provoked by ischemia in certain regions of the heart can be investigated [64]–[70]. In the present context, this is the so-called forward, or direct, problem. This is of course a very interesting subject in itself and may provide useful information about the mechanisms responsible for ST shifts.

2) Inversion: In the present text we are focusing on the inverse problem. More specifically, on how to use BSPM recordings and the model (15)-(16) to identify ischemic heart disease. Due to the particular simple structure (17) of the shift h in the transmembrane potential, it is clear that the ischemic region can be computed if we manage to recover h from ECG data.

The approximate recovery of h from ECG data d is accomplished by dividing the left ventricle into 60 subunits and assigning a basis function to each of these units:

$$N_1(x),\, N_2(x), \ldots,\, N_{60}(x),$$

where

$$N_i(x) \approx \begin{cases} 0\text{mV} & x \text{ outside subunit } i, \\ 50\text{mV} & x \text{ inside subunit } i, \end{cases} \tag{18}$$

for $i = 1, 2, \ldots, 60$. We write " $\approx$ " to emphasize that each of these functions also have a transition zone representing the border between the inside and outside of the subunit. This transition zone is needed because (15) involves the gradient of h. Further information about the steepness and extent of this border zone can be found in the next subsection. Equation (18) is strongly linked and motivated by the concept of a *characteristic function* in mathematics. The characteristic function $\mathcal{X}_D$ of a subdomain D, of a larger domain Ω, is a function that is equal to 1 on D and 0 elsewhere. Hence,

$$N_i \approx 50\mathcal{X}_{D_i},$$

where D_i is the domain occupied by subunit i.

The shift in the transmembrane potential is discretized by putting

$$h(x) = \sum_{i=1}^{60} p_i N_i(x) \tag{19}$$

in (15). Our scheme for identifying ischemic zones is based on the output least squares approach. More specifically, assuming that we have e electrodes, we suggest recovering such regions by minimizing the deviation between the ECG data

$$d = (d_1, d_2, \ldots, d_e)$$

and the simulated ST shift on the body surface. Expressed with mathematical symbols, we may write this problem on the form;

$$\min_{p_1,p_2,\ldots,p_{60}} \frac{1}{2}\left\{\sum_{j=1}^{e}[r(y_j)-d_j]^2+\alpha\sum_{i=1}^{60}p_i^2\right\} \tag{20}$$

subject to

$$\int_B \nabla\psi\cdot(\sigma\nabla r)\,dx \tag{21}$$
$$= -\int_H \nabla\psi\cdot\left(\sigma_i\sum_{i=1}^{60}p_i\nabla N_i\right)dx \quad \text{for all } \psi\in V$$

and

$$0\le p_i\le 1 \quad \text{for } i=1,2,\ldots,60. \tag{22}$$

Here, $\alpha>0$ is a regularization parameter and $y_1,y_2,\ldots,y_e$ are the positions of the electrodes. For $\alpha=0$ the problem is known to be severely unstable, and we used the so called L-curve method to estimate an appropriate value for this parameter, see e.g. [71]. The effective numerical solution of optimization problems of the kind (20)-(22) is a contemporary research field. We employed a simple penalty method, see Appendix A for details.

Simulations were performed with both transmural and subendocardial setups;

- the support of N_i, for $i=1,2,\ldots,60$, occupied the entire heart volume from endocardium to epicardium for transmural lesions,
- subendocardial ischemic regions were represented by letting the support of N_i, for $i=1,2,\ldots,60$, constitute a certain percentage ($<$ 100 %) of the endocardium-epicardium distance, cf. the next subsection.

Consequently, for each patient we obtain two inverse solutions, one using the apriori assumption that the lesion is transmural and one resulting from the assumption that the ischemic area is subendocardial. For these two solutions we computed the deviation, using the standard Euclidean norm, between their associated simulated BSPMs and the clinical BSPM. If the subendocardial simulation produced the least deviation, then the case was classified as subendocardial, otherwise transmural. This classification can thus be done fully automatically.

G. Forward simulation

In our forward model we have to construct a set of appropriate basis functions (18) to represent the shift h in the transmembrane potential (19). Due to the ill-posedness of the inverse problem, the number of basis functions must be kept low. On the other hand, using too few basis functions may give a coarse representation of the ischemic region. Therefore, two important questions to take into account are:

- How many basis functions are needed?
- How should the support of each basis function be chosen?

To find an appropriate number of basis functions for the problem at hand, we used the trial-and-error method. In short, we solved the forward/inverse problem by using 10, 17, 20, 33, 60 and 65 basis functions for the left ventricle. Based on this study, we found that satisfactory results were obtained by using 60 basis functions (but other choices may also be used). At first glance, the numbers 10, 17, 20, 33, 60 and 65 may seem rather arbitrarily, but there is a reason for this selection. To see why, we must look at how the support of each basis function was chosen.

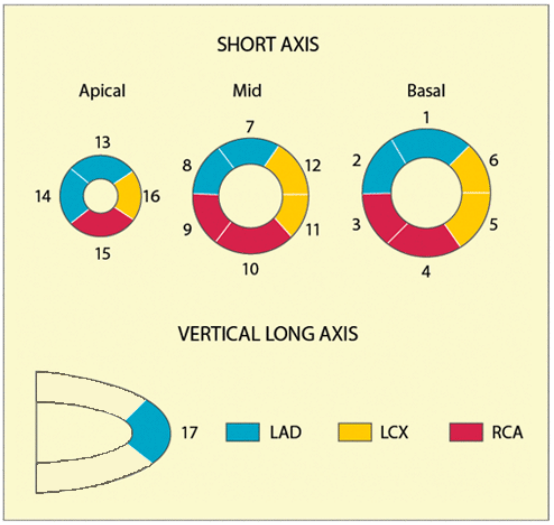

Figure 2. Each of the 17 segments is assigned to one of the three major coronary arteries.

For simulations presented in this paper, the support of each basis function was based on the cardiac anatomy. By doing so, the individual basis function was assigned to specific coronary arterial territories. For years, cardiac imaging modalities have segmented and displayed the heart based on specific coronary arterial territories [72]. The 17 segment model displayed in Figure 2 is commonly used in cardiac imaging. With this model, each segment is assigned to one of the three major coronary arteries: LAD, LCX and RCA. We used a similar assignment for the basis functions in (19). Using 17 basis functions, the support of basis functions 1 to 17 equaled segments 1 to 17, respectively, in Figure 2.

Now, for simulations using a reduced or increased number of basis functions, we merged or split the support of the basis functions based on the coronary arterial territories, see Table I. When the Basal, Medial and Apical regions of the heart (and apex) were divided into finer segments, the division was not done in the Basal-Apex direction, nor did we divide segments in the epicardium-endocardium direction. The division was only done in the angular direction.

Independent of the refinement level, each basis function in Table I was constructed with a smooth boarder zone separating the healthy and ischemic tissue). It has been reported that the transition zone is rather narrow [73], [74]. We have earlier [43], in a pure synthetic setting, investigated the robustness of the present inverse ECG problem with respect to the width of this zone, and we concluded that the solution of the problem is quite robust with respect to this parameter[4]. Based on the

[4]In [43] a level set framework was used to represent the ischemic region, but the stability results can be transfered to the present setting.

Table I
NUMBER OF BASIS FUNCTIONS (= NUMBER OF SEGMENTS) AND THEIR SUPPORT IN THE LEFT VENTRICLE. IT IS STANDARD TO USE 17 SEGMENTS, BUT IN THIS STUDY WE, IF NOT EXPLICITLY STATED OTHERWISE, EMPLOYED 60 SEGMENTS, I.E. 60 BASIS FUNCTIONS.

Number of basis functions	Basal	Medial	Apical	Apex
10	3	3	3	1
17	6	6	4	1
20	6	6	4	4
33	12	12	8	1
60	18	18	12	12
65	24	24	16	1

Table II
A QUANTITATIVE COMPARISON OF ISCHEMIC REGIONS IDENTIFIED BY PERFUSION SCINTIGRAPHY AND BY SOLVING THE INVERSE PROBLEM (20)-(22).

Patient number	Relative difference of center of mass	Relative difference of size: Threshold 0.5	Threshold 0.6
1	9.3%	11.7%	5.0%
2	12.1%	10.0%	13.3%
3	6.6%	3.3%	3.3%
4	15.2%	3.3%	10.0%
Average	10.8% ± 4.4%	7.1% ± 4.6%	7.9% ± 5.4%

findings discussed in [43], we represented the boarder zone in terms of as a linear function, and the transition region occupied approximately 30% of the volume for each direction in space. This choice was also motivated by the fact that if one wants to use a very steep transition, then a very fine computational mesh is needed to obtain the necessary resolution.

As explained at the end of the previous subsection, simulations were performed with both transmural and subendocardial setups. It was simple to perform a transmural simulation since we had constructed the basis functions such that each of them had support in the entire endocardium-epicardium direction. To perform a subendocardial simulation, we first calculated the endocardium-epicardium distance associated with each grid point within the left ventricle. Based on this, the minimum endocardium-epicardium distance could be determined. This distance is defined as md. For subendocardial simulations, the ischemic extension into the heart wall was controlled by restricting the support of each basis function in the endocardium-epicardium direction. The support was now only defined over the region from endocardium and $3/5\ md$ into the heart wall in the endocardium-epicardium direction. With this approach, we had full control over the subendocardial extension, even for varying wall thicknesses.

III. RESULTS

The procedure described above was tested on four patients. More specifically, the parameters $p_1, p_2, \ldots, p_{60}$ in (19) were estimated by solving (20)-(22). Figure 3 shows the results obtained for these patients. The inverse solutions are visualized in terms of a so called bulls eye plot and the coloring of each cell shows the size of the associated $p_i \in [0, 1]$ parameter, see (19). Also the scintigram is depicted in terms of the bulls eye representation of the left ventricle, where the hashed regions represent zones with reversible perfusion defects.

For patients 1, 2 and 4 the inverse solution estimated the ischemic region to be subendocardial, whereas the lesion for patient 3 was classified as transmural. As mentioned above, our scheme does this classification fully automatically by solving the inverse problem (20)-(22) twice, see the discussion at the end of Section II-F for details.

Table II contains a quantitative comparison of the two modalities:

- The relative difference between the center of mass, of the lesions suggested by the two imaging techniques, varies from 6.6% to 15.2% with arithmetic average $10.8\% \pm 4.4\%$.
- The ischemic zones are represented by hashed regions in the images taken with perfusion scintigraphy, i.e. each pixel of the images is either classified as being associated with a point in the heart with completely normal perfusion or with completely abnormal perfusion. That is, a threshold procedure has been used. In order to obtain a reasonable comparison of the volumes of the lesions identified by the two imaging techniques, a similar threshold procedure must be applied to the results generated by solving the inverse ECG problem. This was accomplished as follows:
  - First, the inverse solution was mapped onto the unit interval $[0, 1]$ by a linear map, with 0 and 1 corresponding to zero and full ST shifts, respectively.
  - Thereafter, each subunit was classified as *ischemic* if its associated (mapped) parameter was larger than a certain threshold value T, otherwise the subunit was identified as *normal*.
  - Table II contains results with threshold $T = 0.50$ and threshold $T = 0.60$.

  With $T = 0.50$ the arithmetic average of the differences between the size of the ischemic regions suggested by perfusion scintigraphy and by inverse ECG is $7.1\% \pm 4.6\%$. For $T = 0.60$ this arithmetic average is approximately of the same size, i.e. $7.9\% \pm 5.4\%$. Nevertheless, for each patient, using a threshold $T = 0.60$, instead of $T = 0.50$, has a rather significant influence on the estimated size of the affected area.

For each of the inverse solutions, we also computed the correlation coefficient between the simulated and measured BSPMs. Table III contains these numbers for patients 1-4. More specifically, let

$$d_{\text{true}} = (d_1,\, d_2, \ldots, d_e)$$

and

$$d_{\text{sim}} = (s_1,\, s_2, \ldots, s_e)$$

denote the recorded and simulated BSPMs, respectively, where $e = 72$ is the number of electrodes on the body surface of the patient. The simulated BSPM, d_{sim}, is computed by solving the inverse problem (20)-(22) and thereafter defining

$$s_j = r(y_j) \quad \text{for } j = 1,\, 2, \ldots, e.$$

Table III reports the correlation coefficient between d_{true} and d_{sim} for each of the four patients. This table also contains the

root-mean-square-errors (RMSE):

$$\sqrt{\frac{\sum_1^e (s_i - d_i)^2}{e}}.$$

A. Robustness

The sensitivity of the solution of the inverse problem (20)-(22) with respect to some of the model parameters was investigated.

Simulations with 40mV and 60mV shifts $h(x)$ in the transmembrane potential, instead of 50mV, were performed, see equation (17). This only resulted in a constant scaling of the inverse solutions depicted in the left column in Figure 3. For example, the inverse solution generated by employing a 40mV shift for patient 1 is identical to what is shown in the left panel, in the first row, in Figure 3, expect that the entire solution is multiplied by a constant approximately equal to $40/50 = 0.8$.

For the inverse solutions presented above, the left ventricle was divided into 60 subunits. Inverse solutions were also computed with 33 and 17 subunits, and the results obtained for patient 1 with these discretizations are shown in Figure 4. Qualitatively, the results are similar to those obtained with 60 cells, see top left panel in Figure 3. Quantitatively, we found that:

- The relative difference between the center of mass (of the lesions) computed with 60 and 33 subunits is 2.2%.
- The relative difference between the center of mass (of the lesions) computed with 60 and 17 subunits is 2.0%.
- The range of the inverse solution decreases as the number of cells increases. For example, the range in panel (b) in Figure 4 is $(0.0, 0.655)$, whereas in the top left panel in Figure 3 the range is $(0.0, 0.136)$.

We investigated whether changes in the assumed "thickness" of the subendocardial lesions had any significant impact on the inverse solutions. More precisely, the simulations discussed above employed an assumption of 3/5 subendocardial "thickness". That is, the ischemic region occupied 3/5 of the entire endocardial-epicardial distance. Changing this "thickness" from 3/5 to 1/5 or 4/5 did not cause any significant qualitative changes in the inverse solutions, and the number of subunits classified as ischemic was almost unchanged. Quantitatively, we observed, for example, that for patient 1:

- The relative difference between the center of mass (of the lesions) computed with 3/5 "thickness" and 1/5 "thickness" is 1.7%.
- The relative difference between the center of mass (of the lesions) computed with 3/5 "thickness" and 4/5 "thickness" is 1.5%.

We also explored whether it was necessary to impose inequality constraints on the parameters $p_1, p_2, \ldots, p_{60}$, see (22). For each of the four patients, inverse solutions with and without such constraints were compared. Figure 5 shows such a comparison for patient 3, which was the case that was most influenced by the inequalities. We observe that, if the constraints (22) are omitted, then many of the parameters $p_1, p_2, \ldots, p_{60}$, which constitute the inverse solution, may become less than zero.

Table III
CORRELATION COEFFICIENT AND RMSE BETWEEN RECORDED AND SIMULATED BSPMS

Patient number	1	2	3	4
Correlation coefficient	0.81	0.95	0.85	0.90
RMSE	0.03	0.04	0.04	0.04

Finally, a number of rather extreme tests were undertaken: The BSPM of each patient was employed to compute inverse solutions on the geometries of the other patients. That is, completely "alien" geometrical models were used. The results are presented in [75], and they reveal that the methodology is quite robust with respect changes in the geometrical model of the patient.

IV. DISCUSSION

We have explored the possibilities for using the bidomain model and body surface potential maps to compute the location and size of ischemic regions in the human heart. The results obtained by solving the inverse problem were compared with scintigraphic images. The main focus was on testing a previously published algorithm on clinical data. In earlier studies, this method has been reported to work well on synthetic cases.

Our approach is not based on the classical inverse problems of electrocardiography, which employ the epicardial voltage distribution or the activation sequences as sources for abnormalities observed in the ECGs. Instead, we use the bidomain theory to obtain a model which allows full wall inversion. That is, the inverse solution enables us to classify the lesions as subendocardial or transmural.

For three of the four patients analyzed in this study, namely patients 1, 2 and 3, the two modalities, inverse ECG and perfusion scintigraphy, produced pictures that are qualitatively similar; see the three first rows in Figure 3. The results obtained for patient 4, visualized in the last row in Figure 3, are somewhat more inconclusive; both imaging techniques identify a perfusion defect laterally, but the anteroseptal region present in the scintigram is not that pronounced in the inverse ECG analysis.

From a quantitative perspective, one might argue that the images generated by inverse ECG match quite well with those obtained with perfusion scintigraphy. In fact, the average relative difference between the center of mass of the lesions, estimated by the two modalities, was $10.8\% \pm 4.4\%$. Moreover, the average difference in size of the computed ischemic regions was $7.1 \pm 4.6\%$. Further details can be found in Table II.

According to Table III, both the correlation coefficient and the root-mean-square-error between the simulated and recorded ECGs/BSPMs are good for all four patients - including patient 4. Furthermore, and in contrast to what has been observed in pure in silico studies [45], inequality constraints are needed to get acceptable results, see Figure 5. More specifically:

- From the derivation presented in Section II-F it follows that the variables $p_1, p_2, \ldots, p_{60}$, cf. equation (19), must satisfy

$$p_i \geq 0 \quad \text{for } i = 1, 2, \ldots, 60.$$

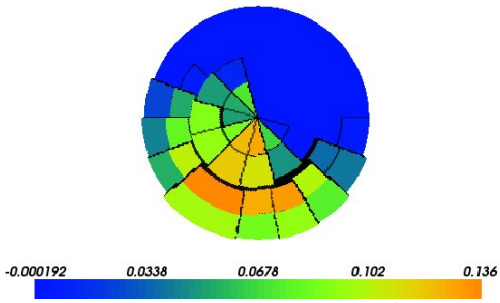

(a1) Patient 1, inverse solution

(b1) Patient 1, scintigram

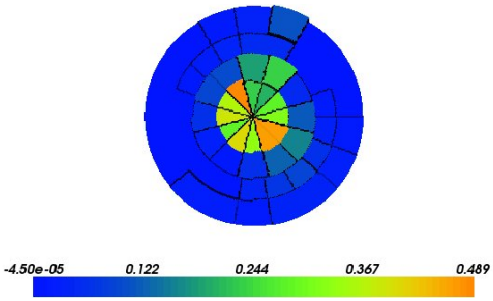

(a2) Patient 2, inverse solution

(b2) Patient 2, scintigram

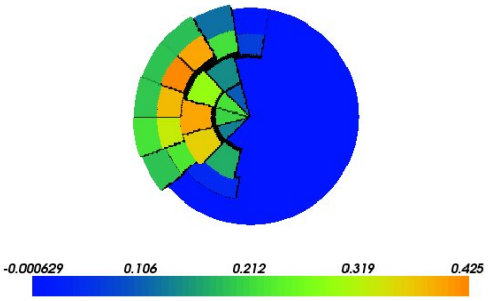

(a3) Patient 3, inverse solution

(b3) Patient 3, scintigram

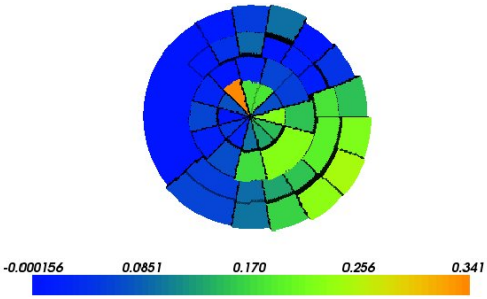

(a4) Patient 4, inverse solution

(b4) Patient 4, scintigram

Figure 3. Panels (a1)-(a4) and (b1)-(b4) show bulls eye plots of the inverse solutions and scintigrams, respectively, for the four patients involved in this study. The inverse solutions are visualized in terms of the parameters p_1, $p_2, \ldots, p_{60}$ employed to discretize the shift in the transmembrane potential, see (19) and (20)-(22). Since the basis functions $\{N_i\}$ have the unit mV, the parameters $\{p_i\}$ do not have any unit, see (18)-(19). The hashed regions in the scintigrams show the areas with significantly reduced perfusion, i.e. classified by the scanner as (reversible) ischemic. (The coloring used in the scintigrams visualizes the degree of perfusion, with white corresponding to 100% perfusion. This coloring is not important in the present study because we focus on the regions with reversible perfusion defects, i.e. the hashed regions.)

This criterion is not fulfilled by the solution shown in the left panel in Figure 5. Hence, the inequality constraints

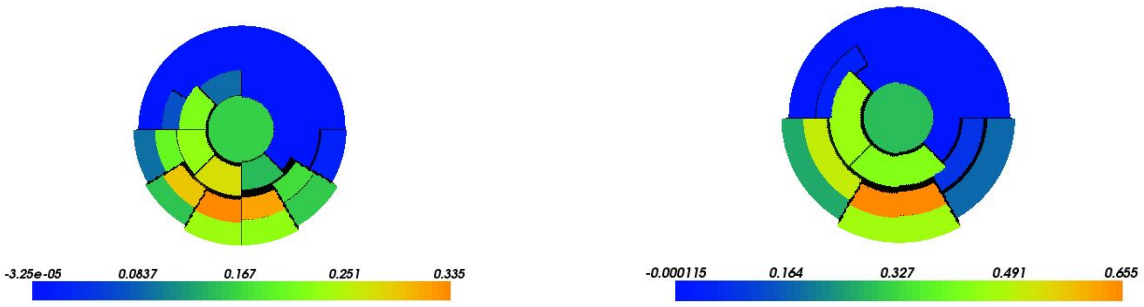

(a) 33 subunits (b) 17 subunits

Figure 4. Inverse solutions computed for patient 1 with 33 subunits (a) and 17 subunits (b). These figures should be compared with the top left panel in Figure 3, which shows the result obtained with 60 subunits.

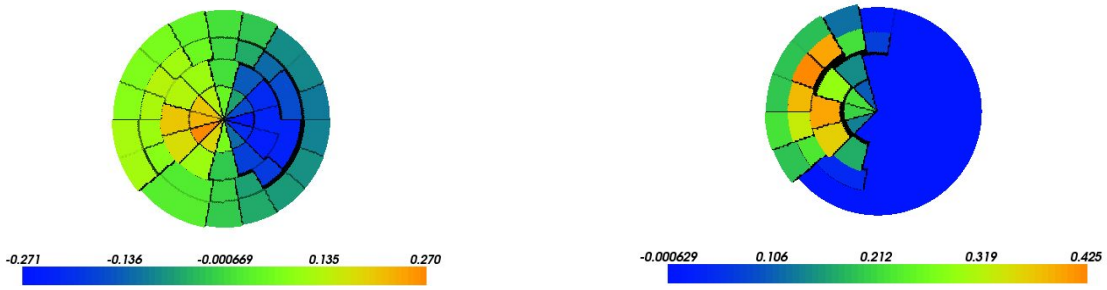

(a) Inverse solution without inequality constraints (b) Inverse solution with inequality constraints

Figure 5. Effects of inequality constraints on the inverse solutions. These are the results obtained for Patient 3. The scintigram from this patient is shown in the right panel in the third row in Figure 3. The correlation coefficients between the simulated and recorded ECGs are 0.91 and 0.85 for the images depicted in (a) and (b), respectively.

(22) are needed in order to obtain inverse solutions that are medically meaningful. This was, to a varying degree, observed for all four patients.

- We observe that the correlation coefficient between the simulated and recorded BSPMs is improved if the inequality constraints are removed from the inverse problem (20)-(22), cf. the caption of Figure 5. From a mathematical point of view, this is not surprising: Removing (22) implies that the cost functional (20) is minimized with fewer constraints, which of course will lead to a solution yielding a smaller value for the cost functional. Apparently, deleting the inequality constraints also provides a better correlation coefficient.

The robustness of the scheme studied in this paper was investigated, and a number of model parameters were perturbed. Changing the assumed shift in the transmembrane potential, caused by the presence of ischemic heart disease, only lead to a constant scaling of the entire inverse solution. This can also be verified from a mathematical point of view.

Reducing the number of subunits, employed to discretize the left ventricle, did not qualitatively alter the results, and the change in the center of mass of the estimated lesions were moderate. Nevertheless, the range of the inverse solutions decreased as the number of subunits were increased. The latter phenomenon can be explained in a rather straightforward manner:

- The projective regularization is weakened on finer partitions, and consequently, more Tikhonov regularization is needed. For the results presented in Figure 4 and in the top left panel in Figure 3, the L-curve method estimated the parameter values $\alpha = 0.0080$ and $\alpha = 0.056$ with 17 and 60 subunits, respectively - a significant increase of the Tikhonov regularization parameter.
- Clearly, minimizing the cost functional (20) is a compromise between making the deviation between the measured and simulated BSPMs small and to determine a solution that has a small Euclidean norm. Furthermore, as α grows, the term

$$\alpha \sum p_i^2$$

"pushes" the solution $(p_1, p_2, \ldots)$ of (20)-(22) towards zero.
- In short, if the number of subunits is increased, then α increases which "pushes" the solution of the inverse problem towards zero. This explains why the range of the inverse solutions on fine partitions (of the left ventricle of the heart) is smaller, compared with results computed on coarser meshes.

Our inverse ECG methodology turned out to be rather robust with respect to uncertainties concerning the apriori assumed "thickness" of subendocardial ischemic regions - both qualitatively and quantitatively. This can probably be explained by the fact that changing this "thickness" only causes the associated synthetic-forward-BSPMs to change in magnitude, not in shape. But the subject definitely needs to be thoroughly investigated.

A series of rather extreme tests were undertaken: The BSPM of each patient was used on the geometries of the other patients, i.e. not using patient specific meshes. According to the results published in [75], these tests indicate, or at least give hope, that patient specific models might not be needed in the clinical setting. However, this issue must be much more thoroughly analyzed.

In spite of these rather positive observations, the present study also has its limitations:

- The algorithm was only tested on four patients.
- We only considered ischemic regions in the left ventricle of the myocardium.
- Our methodology can distinguish between subendocardial and transmural lesions. This classification, however, is performed by employing a "brute-force" approach, i.e. by computing two inverse solutions and choosing the solution which yields the least deviation from the clinical BSPM. We have not explored whether the subendocardial "thickness" can be estimated. In fact, our experiments indicate that this might be difficult: We observed that the inverse solutions computed with, apriori defined, thickness 3/5 (of the endocardial-epicardial distance) were quantitatively rather similar to those obtained with 1/5 and 4/5 thickness. The issue must be thoroughly analyzed.
- We maximally used 60 subunits in the partitioning of the left ventricle. Ideally, one might want to employ finer resolutions. However, this is a subtle issue: We used 72 electrodes on the body surface, and, in the clinical setting, data recorded at some of these electrodes can not be used due to the amount of noise in the signals. Consequently, employing more than 60 subunits will typically lead to a model with more variables than equations, i.e. a underdetermined linear system. In such cases, the associated forward operator will have a nontrivial null space. It is therefore questionable whether dividing the heart into more than, approximately, 60 subunits is a good strategy, unless further electrodes are used. In any case, increasing the number of sub cells will make the problem more ill posed, i.e. more unstable.
- In order to estimate the size of the ischemic region, we employed a threshold procedure. The threshold parameter T, of course, influenced the computed volume. Based on results from four patients only, it is not possible to estimate the "correct" value for T. Far more tests and comparisons with several modalities are needed. An issue closely related to this problem, is the observation that the range of the inverse solution decreases as the number of subunits, used in the partitioning of the heart, increases. Even though this matter is easily explained from a mathematical point of view, the threshold algorithm must be designed to tackle it.
- In addition to ST shifts, which is the main focus of the present study, ischemic heart disease is well known to cause shortening of action potential duration (APD). This effect can not be included in our framework because we consider a stationary model. In fact, if one wants to consider changes in the APD, using the bidomain equations, then one needs to use the complete model (1)-(3). As mentioned above, for inverse solution purposes, this is currently not possible, but, due to the steadily increasing computing power and the development of numerical mathematics, this might become an attractive alternative during the next two decades.
- In this investigation we used a rather simple geometrical model of the patients, i.e. only the lungs and the ventricles where included. The remaining part of the body was treated as a homogeneous bulk. Previous studies, focusing on the forward problem, suggest that also other organs will have a significant impact on the simulated BSPM, see [55] and references therein. The effect of including further organs in our model should therefore be explored. Nevertheless, this is a very subtle issue because the noise in the BSPM recordings might make it difficult to obtain better results with a more sophisticated model. We conclude that an in-depth study is needed.
- In clinical practice, the need for patient specific geometrical models would constitute a severe limitation, and the feasibility of using standardized geometries must therefore be studied. Optimization of the electrode number and placement will also be important for clinical usability [76].
- Myocardial scintigraphy and ECG measure two different sides of exercise-induced, reversible, ischemic myocardial injury; relative differences in myocardial perfusion and ionic fluxes inside the myocardium, respectively. Both methods have their own methodological problems and confounders. Thus, we do not know the absolute truth about the degree and extent of the injury. We only have two methods that indirectly say something about the injury.

In view of this discussion, it seems reasonable to conclude that our results are promising and may serve as the first steps towards validating an imaging technique based on solving the inverse problem of electrocardiography. A large scale validation is needed to further assess the clinical value of the method, both in terms of locating and estimating the size of the ischemic injury, and in terms of diagnostic thresholding, sensitivity and specificity. Such a study must include a healthy control group and preferably further modalities, e.g. angiography.

APPENDIX

A. Penalty method

For implementational simplicity, we decided to use a penalty method for the numerical solution of (20)-(22). Since the heart was divided into only 60 subunits, this scheme turned out to be fast enough.

The inequality constraints (22) are "removed" from the problem by adding a penalty term to the cost functional (20):

$$\min_{p_1,p_2,\ldots,p_{60}} \frac{1}{2} \qquad \left\{ \sum_{j=1}^{e} [r(y_j) - d_j]^2 + \alpha \sum_{i=1}^{60} p_i^2 \right.$$

$$+\beta \sum_{i=1}^{60} (\max\{0, -p_i\})^2 + \beta \sum_{i=1}^{60} (\max\{0, p_i - 1\})^2 \Bigg\}$$

subject to

$$\int_B \nabla\psi \cdot (\sigma \nabla r)\, dx = -\int_H \nabla\psi \cdot \left(\sigma_i \sum_{i=1}^{60} p_i \nabla N_i \right) dx \quad \text{for all } \psi \in V.$$

Here, β is a large positive constant, and $\beta(\max\{0, -p_i\})^2$ or $\beta(\max\{0, p_i - 1\})^2$ become large if p_i is outside the unit interval $[0, 1]$. We solved this penalized approximation of (20)-(22) with a gradient method (steepest descent).

RESEARCH ETHICS

The present study was approved by the Regional Committee for Medical Research Ethics (permission no. S-07161b) and by the Data Protection Officer at Oslo University Hospital according to the Personal Data Act (permission no. 07/3780). Written informed consent was given by all participants.

ACKNOWLEDGMENT

We would like to thank Kristina Hermann Haugaa, Andreas Abildgaard and Jan Gunnar Fjeld at Oslo University Hospital for providing us with the clinical data that was used in this study. The authors would also like to express their sincere gratitude to the team developing the Fenics software tool. Finally, we would like to thank the referees for excellent comments, which significantly improved this article.

All authors fulfill the Vancouver rules for byline authors, section II.A.1.

REFERENCES

[1] J. L. Anderson, C. D. Adams, E. M. Antman, C. R. Bridges, R. M. Califf, D. E. Casey, W. E. Chavey, F. M. Fesmire, J. S. Hochman, T. N. Levin, A. M. Lincoff, E. D. Peterson, P. Theroux, N. K. Wenger, R. S. Wright, S. C. Smith, A. K. Jacobs, J. L. Halperin, S. A. Hunt, H. M. Krumholz, F. G. Kushner, B. W. Lytle, R. Nishimura, J. P. Ornato, R. L. Page, and B. Riegel, "ACC/AHA 2007 guidelines for the management of patients with unstable angina/non-ST-elevation myocardial infarction," *J Am Coll Cardiol*, vol. 50, pp. 1–1, 2007.

[2] E. M. Antman, D. T. Anbe, P. W. Armstrong, E. R. Bates, L. A. Green, M. Hand, J. S. Hochman, H. M. Krumholz, F. G. Kushner, G. A. Lamas, C. J. Mullany, J. P. Ornato, D. L. Pearle, M. A. Sloan, S. C. Smith, J. S. Alpert, J. L. Anderson, D. P. Faxon, V. Fuster, R. J. Gibbons, G. Gregoratos, J. L. Halperin, L. F. Hiratzka, S. A. Hunt, and A. K. Jacobs, "ACC/AHA guidelines for the management of patients with ST-elevation myocardial infarction," *J Am Coll Cardiol*, vol. 44, pp. 1–1, 2004.

[3] K. Fox, M. A. A. Garcia, D. Ardissino, P. Buszman, P. G. Camici, F. Crea, C. Daly, G. d. Backer, P. Hjemdahl, J. Lopez-Sendon, J. Marco, J. Morais, J. Pepper, U. Sechtem, M. Simoons, K. Thygsen, and E. S. o. C. , "Guidelines on the management of stable angina pectoris; the experts of the european society of cardiology on the management of stable angina pectoris," *Kardiol Pol*, vol. 64, no. 8, pp. 823–880, 2006.

[4] R. J. Gibbons, G. J. Balady, J. T. Bricker, B. R. Chaitman, G. F. Fletcher, V. F. Froelicher, D. B. Mark, B. D. McCallister, A. N. Mooss, M. G. O'Reilly, W. L. Winters, E. M. Antman, J. S. Alpert, D. P. Faxon, V. Fuster, G. Gregoratos, L. F. Hiratzka, A. K. Jacobs, R. O. Russell, and S. C. Smith, "ACC/AHA 2002 guideline update for exercise testing," *J Am Coll Cardiol*, vol. 40, pp. 1531–1540, 2002.

[5] R. M. Fuchs, S. C. Achuff, L. Grunwald, F. C. Yin, and L. S. Griffith, "Electrocardiographic localization of coronary artery narrowings: studies during myocardial ischemia and infarction in patients with one-vessel disease," *Circulation*, vol. 66, pp. 1168–1176, 1982.

[6] M. E. Tavel and C. Shaar, "Relation between the electrocardiographic stress test and degree and location of myocardial ischemia," *Am J Cardiol*, vol. 84, pp. 119–124, 1999.

[7] X. Kang, D. S. Berman, H. C. Lewin, R. Miranda, R. Agafitei, I. Cohen, J. D. Friedman, and G. Germano, "Comparative localization of myocardial ischemia by exercise electrocardiography and myocardial perfusion spect," *J Nucl Cardiol*, vol. 7, pp. 140–145, 2000.

[8] T. H. Hauser, S. Dorbala, A. Sulaiman, and M. F. Di Carli, "Quantitative relation of ST-segment depression during exercise to the magnitude of myocardial ischemia as assessed by single-photon emission computed tomographic myocardial perfusion imaging," *Am J Cardiol*, vol. 94, pp. 703–708, 2004.

[9] J. W. Weinsaft, F. J. Wong, J. Walden, M. Szulc, P. M. Okin, and P. Kligfield, "Anatomic distribution of myocardial ischemia as a determinant of exercise-induced ST-segment depression," *Am J Cardiol*, vol. 96, pp. 1356–1360, 2005.

[10] P. Bogaty, J. Guimond, N. M. Robitaille, L. Rousseau, S. Simard, J. R. Rouleau, and G. R. Dagenais, "A reappraisal of exercise electrocardiographic indexes of the severity of ischemic heart disease: angiographic and scintigraphic correlates," *J Am Coll Cardiol*, vol. 29, pp. 1497–1504, 1997.

[11] P. Bogaty, S. Gavrielides, P. Mure, A. Gaspardone, and A. Maseri, "Duration and magnitude of ST-segment depression during exercise and recovery: a symmetric relation," *Am Heart J*, vol. 129, pp. 666–671, 1995.

[12] A. J. Taylor, M. C. Sackett, and G. A. Beller, "The degree of ST-segment depression on symptom-limited exercise testing: relation to the myocardial ischemic burden as determined by thallium-201 scintigraphy," *Am J Cardiol*, vol. 75, pp. 228–231, 1995.

[13] G. W. Manning, "The electrocardiogram of the 2-step exercise stress test," *Am Heart J*, vol. 54, pp. 823–836, 1957.

[14] H. Hanninen, P. Takala, J. Rantonen, M. Makijarvi, K. Virtanen, J. Nenonen, T. Katila, and L. Toivonen, "ST-T integral and T-wave amplitude in detection of exercise-induced myocardial ischemia evaluated with body surface potential mapping," *J Electrocardiol*, vol. 36, pp. 89–98, 2003.

[15] H. Miyakoda, T. Kinugawa, K. Ogino, M. Mori, A. Endo, M. Kato, T. Kato, S. Osaki, I. Hisatome, and C. Shigemasa, "QRST integral analysis of body surface electrocardiographic mapping for assessing exercise-induced changes in the spatial distribution of local repolarization properties in patients with coronary artery disease and in patients with previous anterior infarction," *J Electrocardiol*, vol. 32, pp. 123–136, 1999.

[16] R. G. Murray, M. P. Watts, D. MacFarlane, A. Irving, J. M. Beattie, A. C. Tweddel, T. D. Lawrie, and P. W. MacFarlane, "On-line computer-assisted exercise mapping," *Cardiology*, vol. 68 Suppl 2, pp. 133–140, 1981.

[17] H. S. Oster, B. Taccardi, R. L. Lux, P. R. Ershler, and Y. Rudy, "Noninvasive electrocardiographic imaging: reconstruction of epicardial potentials, electrograms, and isochrones and localization of single and multiple electrocardiac events," *Circulation*, vol. 96, pp. 1012–1024, 1997.

[18] P. Johnston, Ed., *Computational Inverse Problems in Electrocardiography*. WIT Press, 2001.

[19] A. J. Pullan, M. L. Buist, and L. K. Cheng, *Mathematically Modelling the Electrical Activity of the Heart: From Cell to Body Surface and Back*. World Scientific Publishing Company, 2005.

[20] J. Sundnes, G. T. Lines, X. Cai, B. F. Nielsen, K. A. Mardal, and A. Tveito, *Computing the Electrial Activity in the Heart*. Springer-Verlag, 2006.

[21] Y. Rudy and B. J. Messinger-Rapport, "The inverse problem in electrocardiography: Solutions in terms of epicardial potentials," *Critical Reviews in Biomedical Engineering*, vol. 16, pp. 215–268, 1988.

[22] A. J. Pullan, L. K. Cheng, M. P. Nash, C. P. Bradley, and D. J. Paterson, "Noninvasive electrical imaging of the heart: Theory and model development," *Annals of Biomedical Engineering*, vol. 29, no. 10, pp. 817–836, 2001.

[23] O. Dössel, "Inverse problem of electro- and magnetocardiography: Review and recent progress," *International Journal of Bioelectromagnetism*, vol. 2, no. 2, 2000.

[24] R. S. MacLeod and D. H. Brooks, "Recent progress in inverse problems in electrocardiology," *IEEE Engineering in Medicine and Biology*, vol. 17, no. 1, pp. 73–83, 1998.

[25] Y. Rudy and H. S. Oster, "The electrocardiographic inverse problem," *Critical Reviews in Biomedical Engineering*, vol. 20, pp. 25–45, 1992.

[26] B. Tilg, G. Fischer, R. Modre, F. Hanser, B. Messnarz, M. Schocke, C. Kremser, T. Berger, F. Hintringer, and F. X. Roithinger, "Model-based imaging of cardiac electrical excitation in humans," *IEEE Transactions on Medical Imaging*, vol. 21, no. 9, pp. 1031–1039, 2002.

[27] B. Messnarz, M. Seger, R. Modre, G. Fischer, F. Hanser, and B. Tilg, "A comparison of noninvasive reconstruction of epicardial versus transmembrane potentials in consideration of the null space," *IEEE Transactions on Biomedical Engineering*, vol. 51, no. 9, pp. 1609–1618, 2004.

[28] G. Huiskamp and F. Greensite, "A new method for myocardial activation imaging," *IEEE Transactions on Biomedical Engineering*, vol. 44, no. 6, pp. 433–446, 1997.

[29] F. Greensite, "Myocardial activation imaging," in *Computational inverse problems in electrocardiography*, P. Johnston, Ed. WIT Press, 2001, pp. 143–190.

[30] R. Modre, B. Tilg, G. Fischer, and P. Wach, "Noninvasive myocardial activation time imaging: a novel inverse algorithm applied to clinical ECG mapping data," *IEEE Transactions on Biomedical Engineering*, vol. 49, no. 10, pp. 1153–1161, 2002.

[31] L. K. Cheng, J. M. Bodely, and J. Pullan, "Comparison of potential- and activation-based formulations for the inverse problem of electrocardiology," *IEEE Transactions on Biomedical Engineering*, vol. 50, no. 1, pp. 11–22, 2003.

[32] A. Ghodrati, F. Calderero, D. H. Brooks, G. Tadmor, and R. MacLeod, "A level set algorithm for the inverse problem of electrocardiography." Proceedings of 38th Asilomar Conference on Signals, Systems and Computers. November 7-10, 2004. Monterrey, California, USA., 2004.

[33] C. Ramanathan, R. N. Ghanem, P. Jia, K. Ryu, and Y. Rudy, "Noninvasive electrocardiographic imaging for cardiac electrophysiology and arrhythmia," *Nature Med*, vol. 10, pp. 422–428, 2004.

[34] S. Ghosh and Y. Rudy, "Application of L1-norm regularization to epicardial potential solution of the inverse electrocardiography problem," *Annals of Biomedical Engineering*, vol. 37, pp. 902–912, 2009.

[35] T. Berger, B. Pfeifer, F. F. Hanser, F. Hintringer, G. Fischer, M. Netzer, T. Trieb, M. Stuehlinger, W. Dichtl, C. Baumgartner, O. Pachinger, and M. Seger, "Single-beat noninvasive imaging of ventricular endocardial and epicardial activation in patients undergoing CRT," *PLoS ONE*, 2011.

[36] P. S. Cuculich, Y. Wang, B. D. Lindsay, M. N. Faddis, R. B. Schuessler, D. R. J., L. Li, and Y. Rudy, "Noninvasive characterization of epicardial activation in humans with diverse atrial fibrillation patterns," *Circulation*, vol. 122, pp. 1364–1372, 2010.

[37] P. S. Cuculich, J. Zhang, Y. Wang, K. A. Desouza, R. Vijayakumar, P. K. Woodard, and y. Yoram Rudy, "The electrophysiological cardiac ventricular substrate in patients after myocardial infarction: Noninvasive characterization with electrocardiographic imaging," *Journal of the American College of Cardiology*, vol. 58, no. 18, pp. 1893–1902, 2011.

[38] C. Han, Z. Liu, X. Zhang, S. M. Pogwizd, and B. He, "Noninvasive three-dimensional cardiac activation imaging from body surface potential maps: a computational and experimental study on a rabbit model," *IEEE Trans. Med. Imaging*, vol. 27, pp. 1622–1630, 2008.

[39] C. Han, S. M. Pogwizd, C. R. Killingsworth, and B. He, "Noninvasive reconstruction of the three-dimensional ventricular activation sequence during pacing and ventricular tachycardia in the canine heart," *Am. J. Physiol. Heart. Circ. Physiol.*, vol. 302, pp. H244–H252, 2012.

[40] R. S. MacLeod, M. Gardner, R. M. Miller, and B. M. Horacek, "Application of an electrocardiographic inverse solution to localize ischemia during coronary angioplasty," *J Cardiovasc Electrophysiol*, vol. 6, pp. 2–18, 1995.

[41] J. E. Burnes, B. Taccardi, R. S. MacLeod, and Y. Rudy, "Noninvasive ECG imaging of electrophysiologically abnormal substrates in infarcted hearts : A model study," *Circulation*, vol. 101, pp. 533–540, 2000.

[42] G. Li and B. He, "Noninvasive estimation of myocardial infarction by means of a heart-model-based imaging approach: a simulation study," *Med. Biol. Eng. Comput.*, vol. 42, pp. 128–136, 2004.

[43] B. F. Nielsen, O. M. Lysaker, and A. Tveito, "On the use of the resting potential and level set methods for identifying ischemic heart disease; an inverse problem," *Journal of Computational Physics*, vol. 220, no. 2, pp. 772–790, 2007.

[44] M. C. MacLachlan, B. F. Nielsen, O. M. Lysaker, and A. Tveito, "Computing the size and location of myocardial ischemia using measurements of ST-segment shift," *IEEE Transactions on Biomedical Engineering*, vol. 53, no. 6, pp. 1024–1031, June 2006.

[45] B. F. Nielsen, X. Cai, and O. M. Lysaker, "On the possibility for computing the transmembrane potential in the heart with a one shot method; an inverse problem," *Mathematical Biosciences*, vol. 210, no. 2, pp. 523–553, 2007.

[46] M. Burger, K. A. Mardal, and B. F. Nielsen, "Stability analysis of the inverse transmembrane potential problem in electrocardiography," *Inverse Problems*, vol. 26, no. 10, 2010.

[47] D. Wang, R. M. Kirby, R. S. MacLeod, and C. R. Johnson, "Inverse electrocardiographic source localization of ischemia: an optimization framework and finite element solution," *under review*, 2011.

[48] B. He, G. Li, and X. Zhang, "Noninvasive imaging of cardiac transmembrane potentials within three-dimensional myocardium by means of a realistic geometry anisotropic heart model," *IEEE Transactions on Biomedical Engineering*, vol. 50, no. 10, pp. 1190–1202, 2003.

[49] B. He and C. Liu, "Cardiac electrophysiological imaging-solving the inverse problem of electrocardiography," in *Cardiac Electrophysiology Methods and Models*, D. Sigg, Ed. Springer, 2010.

[50] X. Zhang, I. Ramachandra, Z. Liu, B. Muneer, S. M. Pogwizd, and B. He, "Noninvasive three-dimensional electrocardiographic imaging of ventricular activation sequence," *Am. J. Physiol. Heart. Circ. Physiol.*, vol. 289, pp. H2724–2732, 2005.

[51] C. Liu, M. Eggen, C. Swingen, P. A. Iaizzo, and B. He, "Noninvasive mapping of transmural potentials during activation in swine hearts from body surface electrocardiograms," *IEEE Transactions on Medical Imaging*, vol. 31, pp. 1777 – 1785, 2012.

[52] BioSemi Website. BioSemi B.V. Amsterdam, Netherlands. [Online]. Available: http://www.biosemi.com

[53] G. Farin, *Curves and Surfaces for Computer-Aided Geometric Design: A Practical Guide*. Academic Press, 1988.

[54] Tetmesh, "Tetmesh ghs3d," http://www.distene.com.

[55] U. J. Keller, F. M. Weber, G. Seemann, and O. Dössel, "Ranking the influence of tissue conductivities on forward-calculated ECGs," *IEEE Transactions on Biomedical Engineering*, vol. 57, no. 7, pp. 1568–1576, 2010.

[56] P. M. F. Nielsen, I. J. L. Grice, B. H. Smaill, and P. J. Hunter, "Mathematical model of geometry and fibrous structure of the heart," *American Journal of Physiology*, vol. 260, pp. 1365–1378, 1991.

[57] G. Seemann, D. U. J. Keller, D. L. Weiss, and O. Dössel, "Modeling human ventricular geometry and fiber orientation based on diffusion tensor MRI," *Proc. Computers in Cardiology*, vol. 33, pp. 801–804, 2006.

[58] O. M. Lysaker and B. F. Nielsen, "Towards a level set framework for infarction modeling: An inverse problem," *International Journal of Numerical Analysis and Modeling*, vol. 3, no. 4, pp. 377–394, 2006.

[59] J. Keener and J. Sneyd, *Mathematical Physiology*. Springer-Verlag, 1998.

[60] T. D. Barrett, B. A. MacLeod, and M. J. Walker, "A model of myocardial ischemia for the simultaneous assessment of electrophysiological changes and arrhythmias in intact rabbits." *J Pharmacol Toxicol Methods*, vol. 37, no. 1, pp. 27–36, Feb 1997.

[61] A. G. Kleber, M. J. Janse, F. J. van Capelle, and D. Durrer, "Mechanism and time course of S-T and T-Q segment changes during acute regional myocardial ischemia in the pig heart determined by extracellular and intracellular recordings," *Circulation Research*, vol. 42, pp. 603–613, 1978.

[62] E. Downar, M. J. Janse, and D. Durrer, "The effect of acute coronary artery occlusion on subepicardial transmembrane potentials in the intact porcine heart," *Circulation*, vol. 56, pp. 217–224, 1977.

[63] W. E. Cascio, H. Yang, T. A. Johnson, B. J. Muller-Borer, and J. J. Lemasters, "Electrical properties and conduction in reperfused papillary muscle," *Circulation Research*, vol. 89, pp. 807–814, 2001.

[64] D. Li, C. Y. Li, A. C. Yong, and D. Kilpatrick, "Source of electrocardiographic ST changes in subendocardial ischemia," *Circulation Research*, vol. 82, pp. 957–970, 1998.

[65] F. Hanser, M. Seger, B. Tilg, R. Modre, G. Fisher, B. Messnarz, F. Hintringer, T. Berger, and F. X. Roithinger, "Influence of ischemic and infarcted tissue on the surface potential," *Proc. Computers in Cardiology*, vol. 30, pp. 789–792, 2003.

[66] P. R. Johnston, D. Kilpatrick, and C. Y. Li, "The importance of anisotropy in modeling ST segment shift in subendocardial ischaemia," *IEEE Trans. Biomed. Eng.*, vol. 48, pp. 1366–1376, 2001.

[67] P. R. Johnston and D. Kilpatrick, "The effect of conductivity values on ST segment shift in subendocardial ischaemia," *IEEE Trans. Biomed. Eng.*, vol. 50, pp. 150–158, 2003.

[68] D. Kilpatrick, P. R. Johnston, and D. S. Li, "Mechanisms of ST change in partial thickness ischemia," *J. Electrocardiol.*, vol. 36, pp. 7–12, 2003.

[69] B. Hopenfeld, J. G. Stinstra, and R. S. MacLeod, "A mechanism for ST depression associated with contiguous subendocardial ischemia," *J. Cardiovasc. Electrophysiol.*, vol. 15, pp. 1200–1206, 2004.

[70] M. Wilhelms, O. Dössel, and G. Seemann, "In silico investigation of electrically silent acute cardiac ischemia in the human ventricles," *IEEE Transactions on Biomedical Engineering*, vol. 58, no. 10, pp. 2961–2964, 2011.
[71] P. C. Hansen, *Discrete Inverse Problems: Insight and Algorithms*. SIAM, 2010.
[72] M. Cerqueira, N. Weissman, V. Dilsizian, A. Jacobs, S. Kaul, W. Laskey, D. Pennell, J. Rumberger, T. Ryan, and M. Verani, "Standardized myocardial segmentation and nomenclature for tomographic imaging of the heart," *Circulation, Journal of the American Heart Association*, vol. 105, pp. 539–542, 2002.
[73] M. R. Franz, J. T. Flaherty, E. V. Platia, B. H. Bulkley, and M. L. Weisfeldt, "Localization of regional myocardial ischemia by recording of monophasic action potentials," *Circulation*, vol. 69, pp. 593–604, 1984.
[74] J. D. Hearse, L. H. Opie, I. E. Katzeff, W. F. Lubbe, T. J. Van der Werff, M. Peisach, and G. Boulle, "Characterization of the "border zone" in acute regional ischemia in the dog," *Am J Cardiol.*, vol. 40, no. 5, pp. 716–726, 1977.
[75] O. Lysaker, B. F. Nielsen, and G. P., "On the use of the bidomain model for computing the position and size of ischemic regions; a validation study," *Proc. Computing in Cardiology*, vol. 39, pp. 449–452, 2012.
[76] Y. Jiang, C. Qian, R. Hanna, D. Farina, and O. Dössel, "Optimization of the electrode positions of multichannel ECG for the reconstruction of ischemic areas by solving the inverse electrocardiographic problem," *International Journal of Bioelectromagnetism*, vol. 11, no. 1, pp. 27 – 37, 2009.